Charged bilayer membranes in asymmetric ionic solutions: Phase diagrams and critical behavior

Naofumi Shimokawa*
Institute of Industrial Science, University of Tokyo, Tokyo 153-8505, Japan

Shigeyuki Komura
Department of Chemistry, Graduate School of Science and Engineering, Tokyo Metropolitan University, Tokyo 192-0397, Japan, and Kavli Institute for Theoretical Physics China, CAS, Beijing 100190, China

David Andelman
Raymond and Beverly Sackler School of Physics and Astronomy, Tel Aviv University, Ramat Aviv 69978, Tel Aviv, Israel, and Kavli Institute for Theoretical Physics China, CAS, Beijing 100190, China

(Received 17 May 2011; published 19 September 2011)

We consider the phase separation in an asymmetrically charged lipid bilayer membrane consisting of neutral and negatively charged lipids that are in contact with in and out ionic solutions having different ionic strengths. The two asymmetric leaflets are coupled through electrostatic interactions. Based on a free-energy approach, the critical point and phase diagrams are calculated for different ionic strengths of the two solutions and coupling parameter. An increase of the coupling constant or asymmetry in the salt concentration between the in and out solutions yields a higher phase-separation temperature because of electrostatic interactions. As a consequence, the phase-coexistence region increases for strong screening (small Debye length). Finally, possible three-phase coexistence regions in the phase diagram are predicted.

DOI: 10.1103/PhysRevE.84.031919 PACS number(s): 87.16.D−, 64.60.−i, 64.75.−g

I. INTRODUCTION

Model membranes consisting of mixtures of saturated lipids, unsaturated lipids, and cholesterol have received considerable attention in recent years because they can be regarded as model systems of biological cell membranes. Below a certain temperature, the membrane undergoes a lateral phase separation between a liquid-ordered phase (rich in saturated lipid and cholesterol) and a liquid-disordered phase (rich in unsaturated lipid). The resulting lipid domains are sometimes called "rafts" and are believed to play an important role in various biocellular processes such as signal transduction and cooperative membrane trafficking [1].

A large number of experimental studies have been carried out to further explore the consequences of domain formation in model membranes and their relation with biomembrane functioning. They include, among others, studies of domain morphology [2,3], domain budding [4], growth dynamics of domains [5], and formation of periodic lateral structures [6]. In particular, we note that lateral phase segregation was directly observed for lipids at the air-water interface and for giant lipid vesicles using fluorescence microscopy [2–6]. Furthermore, in an attempt to understand these experimental findings, several theoretical models have been proposed [7–9].

More recently, several experimental works have been conducted in order to understand how electrostatic interactions affect the phase separation of model membranes composed of charged and neutral lipids [10,11]. As charged lipids are ever present in biomembranes, the role of electrostatic interactions is important also for biological cells. The phase-coexistence region was reported to be fully suppressed in lipid bilayers consisting of a three-component mixture of neutral saturated lipid DPPC (1,2-dipalmitoyl-sn-glycero-3-phosphocholine), negatively charged unsaturated lipid DOPS (1,2-dioleoyl-sn-glycero-3-phospho-L-serine), and cholesterol, because of the electrostatic repulsion between charged lipids [10]. Furthermore, the extent of the phase-coexistence region appears when salt ($CaCl_2$) is added, an effect that can be understood by the screening of electrostatic interactions in presence of added salt. In a related experimental study, it was shown that for mixtures of DPPC, negatively charged DOPG (L-α-1,2-dioleoyl-sn-glycero-3-phosphoglycerol) and cholesterol, the phase-separation temperature becomes higher as salt is added [11]. Such effects were also considered in several theoretical studies [12–14].

Another important aspect of biomembranes is the compositional asymmetry between their inner and outer leaflets. Collins and Keller investigated the phase behavior in asymmetric lipid bilayers and showed that the domain formation in each leaflet is coupled through an interleaflet interaction [15]. In some cases it was reported that phase separation in one of the leaflets induces a phase separation in the second leaflet, while in other cases the lack of phase separation in one leaflet suppresses domain formation in the second leaflet. Theoretical models based on regular solution theory [16] or Landau theory [17] attempted to take into account interleaflet interactions and explored their consequences on the bilayer phase diagram.

In related works based on the Poisson-Boltzmann theory, a model describing the immiscibility transition in *asymmetric and charged* membranes was proposed by May and coworkers [18,19]. Their model took into account an interleaflet *electrostatic* coupling between two rigid and charged planes modeling a bilayer membrane. The spinodal line, characterizing the phase coexistence, and the critical point were derived and depend on the ionic strength of the solution as well as on the

*nshimo@iis.u-tokyo.ac.jp

interleaflet electrostatic coupling. One of the main conclusions was that a stronger interleaflet coupling enhances the lateral phase separation. However, it was equally assumed by the authors that the two aqueous solutions in contact with the two leaflets have the same salt concentration. We note that this assumption is an oversimplification for cellular biomembranes, where due to ionic channels and other active processes, the ionic strength is different on the two sides of the membrane (the inner- and extracellular regions). This difference in ionic strength, in turn, contributes to an additional gap between the surface potential on the two sides of the bilayer and plays an important role, for example, in neurotransmission processes.

In the present work, we extend the model of Refs. [18,19] in order to mimic asymmetric biomembranes in a more complete way. In Sec. II we introduce a model based on Poisson-Boltzmann theory to describe phase separation for asymmetric charged bilayers "sandwiched" between two ionic solutions having different ionic strength. In Sec. III the variation of the critical point and the entire phase diagram as a function of the ionic strength (Debye length) and interleaflet electrostatic coupling is explored. It is shown that the phase separation is enhanced as the salt concentration is increased and is due to the enhanced electrostatic screening. When an electrostatic coupling between the leaflets is introduced, the lateral phase separation occurs at higher temperatures as compared with the no-coupling case. We also show that the phase-separation temperature increases when the concentration difference between the two salt reservoirs becomes larger. Finally, discussion and comparison with other works are presented in Sec. IV.

II. MODEL

The system is modeled as a binary lipid-bilayer composed of a mixture of negatively charged and neutral lipids. Although many experiments are done in the presence of added cholesterol as a third component, it is reasonable to stay within the simpler case of a binary lipid mixture. As cholesterol is noncharged, its presence will not change in any major way our predictions on the role of electrostatics.

The bilayer consists of two undeformable and parallel leaflets, lying in the xy plane and in contact, respectively, with the two monovalent salt solutions, as shown in Fig. 1. Let us label all quantities residing on the inner leaflet by the subscript 1 and those on the outer one by 2. The inner leaflet (leaflet 1) is located at $z = d$ and is in contact with the inner reservoir located at $z > d$, while the outer leaflet (leaflet 2) is located at $z = 0$ and is in contact with the outer reservoir at $z < 0$. In some experiments spontaneous budding of charged domains toward the vesicular interior was reported [10]. This can be explained by considering the increase in the osmotic pressure coupled with the change in spontaneous curvature of the outer leaflet. However, in the present study we assume that the bilayer remains flat and neglect the effect of the osmotic pressure generated across the bilayer. Our model is further based on three principal assumptions: (1) Because we do not consider membrane undulations and their curvature, the two leaflets have the same area A. (2) The neutral and negatively charged lipids have the same cross-sectional area per lipid Σ. This is supported by many experiments on fluid-like membranes. (3) Furthermore, each leaflet is taken

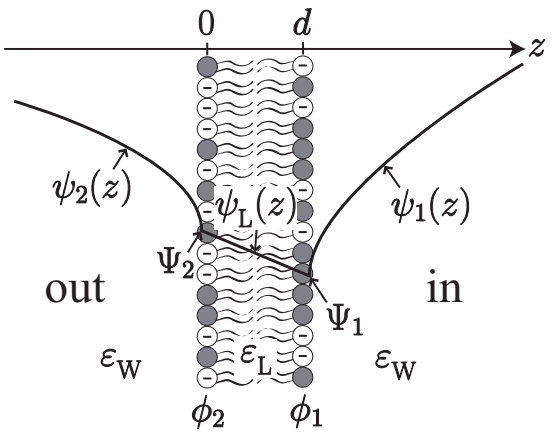

FIG. 1. Schematic representation of the electrostatic potential for a binary lipid bilayer consisting of negatively charged and neutral lipids. The head groups of leaflets 1 and 2 are located at the plane $z = d$ and $z = 0$, respectively. The (dimensionless) electrostatic potentials in solutions 1 ($z > d$) and 2 ($z < 0$) are denoted by $\psi_1(z)$ and $\psi_2(z)$, respectively. The dimensionless surface potentials at the two leaflets are denoted by $\Psi_1 = \psi_1(z = d)$ and $\Psi_2 = \psi_2(z = 0)$, while $\psi_L(z)$ is the (dimensionless) electric potential inside the hydrocarbon core region ($0 \leqslant z \leqslant d$) of the lipid membrane. The dielectric constant of the aqueous region (water) and lipid hydrocarbon core are denoted by ε_W and ε_L, respectively.

as an incompressible two-dimensional fluid. Hence, the two leaflets consist of the same total number of lipid molecules $N = A/\Sigma$.

The total free energy per lipid molecule is given by

$$f_{tot}(\phi_1,\phi_2) = f_{mix}(\phi_1) + f_{mix}(\phi_2) + f_{el}(\phi_1,\phi_2), \qquad (1)$$

where all energies are measured in units of k_BT (k_B is the Boltzmann constant and T the temperature), and ϕ_1 and ϕ_2 are the mole fractions of the negatively charged lipid in leaflets 1 and 2, respectively. The free energy f_{tot} consists of two nonelectrostatic f_{mix} terms (one for each leaflet) and an electrostatic one f_{el} that induces an interleaflet coupling.

The nonelectrostatic f_{mix} is the Flory-Huggins free energy of lateral mixing in each of the leaflets separately:

$$f_{mix}(\phi) = \phi \ln \phi + (1-\phi)\ln(1-\phi) + \chi\phi(1-\phi), \qquad (2)$$

where χ is the (nonelectrostatic) interaction parameter between the two different lipids. Quite generally, χ is taken to vary inversely with the temperature. The free energy f_{mix} is a sum of the ideal entropy and enthalpy of mixing between the two lipid species. In the absence of the electrostatic interaction, $f_{el} = 0$, the two-phase coexistence region in the (χ,ϕ) plane is delimited by a demixing curve that terminates at the critical point: $\chi_c = 2$ and $\phi_c = 0.5$.

The electrostatic free energy f_{el} can be calculated through the charging process [20]:

$$f_{el}(\phi_1,\phi_2) = -\int_0^{\phi_1} \Psi_1(s_1,0)\,ds_1 - \int_0^{\phi_2} \Psi_2(\phi_1,s_2)\,ds_2, \qquad (3)$$

where $\Psi_1 = e\Phi_1(z = d)/k_BT$ and $\Psi_2 = e\Phi_2(z = 0)/k_BT$ are the dimensionless surface potentials on leaflets 1 ($z = d$) and 2 ($z = 0$), respectively, and e is the elementary charge, while the electric potential inside the lipid hydrocarbon core region

$(0 \leqslant z \leqslant d)$ is denoted by $\Phi_{\rm L}(z)$. Within mean-field theory, the electric potential $\Phi(z)$ satisfies the Poisson-Boltzmann equation

$$\frac{d^2\Phi}{dz^2} = \frac{2en}{\varepsilon_{\rm w}} \sinh \frac{e\Phi}{k_{\rm B}T}, \tag{4}$$

where n is the salt concentration in bulk and $\varepsilon_{\rm w}$ the dielectric constant of the aqueous solution (water). Using the dimensionless electrostatic potential $\psi(z) \equiv e\Phi(z)/k_{\rm B}T$, we obtain the following Poisson-Boltzmann equations in regions 1 and 2 for $\psi_{1,2}(z)$, and Laplace equation in the core region for $\psi_{\rm L}(z)$:

$$\begin{aligned} \frac{d^2\psi_1}{dz^2} &= \kappa_1^2 \sinh\psi_1, \quad z > d, \\ \frac{d^2\psi_2}{dz^2} &= \kappa_2^2 \sinh\psi_2, \quad z < 0, \\ \frac{d^2\psi_{\rm L}}{dz^2} &= 0, \qquad\qquad 0 \leqslant z \leqslant d, \end{aligned} \tag{5}$$

where κ_1^{-1} and κ_2^{-1} are the Debye screening length in regions 1 and 2, respectively, defined by $(\kappa_{1,2})^{-1} = \sqrt{\varepsilon_{\rm w} k_{\rm B}T/2e^2 n_{1,2}}$. Using the Gauss theorem, the boundary conditions of the two leaflets are given by

$$\begin{aligned} \varepsilon_{\rm w}\frac{d\psi_1}{dz}\bigg|_{z=d} - \varepsilon_{\rm L}\frac{d\psi_{\rm L}}{dz}\bigg|_{z=d} &= \frac{e^2\phi_1}{k_{\rm B}T\Sigma}, \\ \varepsilon_{\rm w}\frac{d\psi_2}{dz}\bigg|_{z=0} - \varepsilon_{\rm L}\frac{d\psi_{\rm L}}{dz}\bigg|_{z=0} &= -\frac{e^2\phi_2}{k_{\rm B}T\Sigma}, \end{aligned} \tag{6}$$

where Σ is the cross-sectional area per lipid head group and $\varepsilon_{\rm L}$ is the dielectric constant of the lipid hydrocarbon core region. Far from both sides of the membrane, the bulk electric potential is taken to be zero, $\psi_1(z \to \infty) = 0$ and $\psi_2(z \to -\infty) = 0$.

Under these boundary conditions, the above equations can be solved analytically, yielding transcendental expressions for the two surface potentials, Ψ_1 and Ψ_2:

$$\begin{aligned} \Psi_1 &= -2\sinh^{-1}\left(p_1\phi_1 + p_1 H\Delta\Psi\right), \\ \Psi_2 &= -2\sinh^{-1}\left(p_2\phi_2 - p_2 H\Delta\Psi\right), \end{aligned} \tag{7}$$

where $\Delta\Psi = \Psi_1 - \Psi_2$ is the membrane potential gap. Throughout the paper we will make use of three dimensionless quantities defined as

$$\begin{aligned} p_1 &= \frac{2\pi\ell_{\rm B}}{\kappa_1\Sigma} \sim \kappa_1^{-1}, \\ p_2 &= \frac{2\pi\ell_{\rm B}}{\kappa_2\Sigma} \sim \kappa_2^{-1}, \\ H &= \frac{\Sigma}{4\pi\varepsilon_{\rm w}\ell_{\rm B}}\frac{\varepsilon_{\rm L}}{d} \sim \frac{\varepsilon_{\rm L}}{d}, \end{aligned} \tag{8}$$

where $\ell_{\rm B} = e^2/(4\pi\varepsilon_{\rm w}k_{\rm B}T) \simeq 7$ Å is the Bjerrum length. The ratio $p_2/p_1 = \kappa_1/\kappa_2$ is related to the ratio between the two Debye screening lengths $(\kappa_{1,2})^{-1}$ of the two solutions, and H is the rescaled electrostatic coupling parameter between the two leaflets. By further defining $\overline{\phi}_1 \equiv \phi_1 + H\Delta\Psi$ and $\overline{\phi}_2 \equiv \phi_2 - H\Delta\Psi$ as effective mole fractions of the negatively charged lipid in each leaflet, we can rewrite Eq. (7) as

$$\begin{aligned} \Psi_1 &= -2\sinh^{-1}(p_1\overline{\phi}_1), \\ \Psi_2 &= -2\sinh^{-1}(p_2\overline{\phi}_2). \end{aligned} \tag{9}$$

Furthermore, the potential difference across the membrane $\Delta\Psi = \Psi_1 - \Psi_2$ satisfies a transcendental equation

$$\Delta\Psi = -2\sinh^{-1}(p_1\overline{\phi}_1) + 2\sinh^{-1}(p_2\overline{\phi}_2), \tag{10}$$

since $\overline{\phi}_{1,2}$ themselves depend on $\Delta\Psi$ as defined above.

By substituting back the surface potentials, Eq. (7), into Eq. (3), we obtain the final expression of the electrostatic free energy:

$$f_{\rm el}(\phi_1,\phi_2) = \tfrac{1}{2}H(\Delta\Psi)^2 + f_{\rm m}(\overline{\phi}_1) + f_{\rm m}(\overline{\phi}_2). \tag{11}$$

The first term corresponds to the charging energy stored in the two charged leaflets that are analogous to a two-plate capacitor. The second and third terms represent the electrostatic energy of the two isolated charged monolayers. In the absence of the electrostatic coupling between the two leaflets ($H = 0$), $f_{\rm el}$ is simply the sum of the free energies of two isolated leaflets, i.e., $f_{\rm el}(\phi_1,\phi_2) = f_{\rm m}(\phi_1) + f_{\rm m}(\phi_2)$. Within the Poisson-Boltzmann theory, $f_{\rm m}$ was derived in Ref. [21], and we briefly repeat this derivation in the Appendix. The result is

$$\begin{aligned} f_{\rm m}(\overline{\phi}) &= 2\int_0^{\overline{\phi}} \sinh^{-1}(ps)\,ds \\ &= 2\overline{\phi}\left\{\frac{1-\sqrt{(p\overline{\phi})^2+1}}{p\overline{\phi}} + \ln\left[p\overline{\phi} + \sqrt{(p\overline{\phi})^2+1}\right]\right\}, \end{aligned} \tag{12}$$

where $p = p_1$ for $\overline{\phi} = \overline{\phi}_1$, and $p = p_2$ for $\overline{\phi} = \overline{\phi}_2$. We first solve Eq. (10) to obtain $\Delta\Psi$ and then use it to calculate the total free energy from Eqs. (1), (2), (11), and (12).

In order to analyze the membrane stability toward a lateral phase separation, we calculate the spinodal surface given in the (ϕ_1, ϕ_2, χ) parameter space by the condition

$$\left(\frac{\partial^2 f_{\rm tot}}{\partial\phi_1^2}\right)\left(\frac{\partial^2 f_{\rm tot}}{\partial\phi_2^2}\right) - \left(\frac{\partial^2 f_{\rm tot}}{\partial\phi_1\partial\phi_2}\right)^2 = 0. \tag{13}$$

Using the total free energy of Eq. (1), we obtain

$$\begin{aligned} &\left[\frac{1}{\phi_1(1-\phi_1)} - 2\chi + \left(\frac{\partial^2 f_{\rm el}}{\partial\phi_1^2}\right)\right] \\ &\times\left[\frac{1}{\phi_2(1-\phi_2)} - 2\chi + \left(\frac{\partial^2 f_{\rm el}}{\partial\phi_2^2}\right)\right] = \left(\frac{\partial^2 f_{\rm el}}{\partial\phi_1\partial\phi_2}\right)^2. \end{aligned} \tag{14}$$

The first and second derivatives of the electrostatic free energy, $f_{\rm el}(\phi_1,\phi_2)$, are given by Eq. (11) and can be expressed as

$$\begin{aligned} \frac{\partial f_{\rm el}}{\partial\phi_1} &= 2\sinh^{-1}(p_1\overline{\phi}_1) = -\Psi_1, \\ \frac{\partial f_{\rm el}}{\partial\phi_2} &= 2\sinh^{-1}(p_2\overline{\phi}_2) = -\Psi_2, \end{aligned} \tag{15}$$

and

$$\begin{aligned} \frac{\partial^2 f_{\rm el}}{\partial\phi_1^2} &= \frac{f_{\rm m}''(\overline{\phi}_1) + Hf_{\rm m}''(\overline{\phi}_1)f_{\rm m}''(\overline{\phi}_2)}{1 + H[f_{\rm m}''(\overline{\phi}_1) + f_{\rm m}''(\overline{\phi}_2)]}, \\ \frac{\partial^2 f_{\rm el}}{\partial\phi_2^2} &= \frac{f_{\rm m}''(\overline{\phi}_2) + Hf_{\rm m}''(\overline{\phi}_1)f_{\rm m}''(\overline{\phi}_2)}{1 + H[f_{\rm m}''(\overline{\phi}_1) + f_{\rm m}''(\overline{\phi}_2)]}, \end{aligned}$$

$$\frac{\partial^2 f_{\rm el}}{\partial\phi_1\partial\phi_2} = \frac{H f_{\rm m}''(\bar{\phi}_1) f_{\rm m}''(\bar{\phi}_2)}{1 + H[f_{\rm m}''(\bar{\phi}_1) + f_{\rm m}''(\bar{\phi}_2)]}, \tag{16}$$

where $f_{\rm m}''(\bar{\phi}) = d^2 f_{\rm m}(\bar{\phi})/d\bar{\phi}^2 = 2p/\sqrt{(p\bar{\phi})^2+1}$. Finally, the spinodal surface $\chi_{\rm sp}(\phi_1,\phi_2)$ for fixed p_1, p_2, H can be determined according to Eqs. (10), (14), and (16).

The chemical potential is a function of the lipid concentration

$$\begin{aligned}\mu_1 &= \frac{\partial f_{\rm tot}}{\partial\phi_1} = 2\sinh^{-1}(p\bar{\phi}_1) + \ln\frac{\phi_1}{1-\phi_1} + \chi(1-2\phi_1),\\ \mu_2 &= \frac{\partial f_{\rm tot}}{\partial\phi_2} = 2\sinh^{-1}(p\bar{\phi}_2) + \ln\frac{\phi_2}{1-\phi_2} + \chi(1-2\phi_2).\end{aligned} \tag{17}$$

Under the assumptions mentioned at the beginning of this section, the condition for phase coexistence (the binodal line) requires the equality of the chemical potential of the two phases, A and B, on each of the two leaflets, meaning that both $\mu_{1,\rm A} = \mu_{1,\rm B}$ and $\mu_{2,\rm A} = \mu_{2,\rm B}$ should be simultaneously satisfied on the two leaflets. In addition, the thermodynamic potential

$$g(\phi_1,\phi_2) = f_{\rm tot}(\phi_1,\phi_2) - \mu_1\phi_1 - \mu_2\phi_2 \tag{18}$$

should be equal for the two phases, i.e, $g_{\rm A} = g_{\rm B}$. These conditions are sufficient to calculate the two-phase coexistence region as well as the corresponding tie lines inside the coexistence region, as will be discussed below in Sec. III. We remark that the same conditions were also used in previous works [16,17].

A. The symmetric in and out reservoir case, $p_1 = p_2$

Let us first discuss the case of equal ionic strength ($p_1 = p_2$) of the two solutions and review some of the results reported already in Ref. [18]. The critical point, because of the in and out symmetry, is located on the $\phi_1 = \phi_2$ line, and the expression for the spinodal line is given by

$$\chi_{\rm sp} = \frac{1}{2\phi(1-\phi)} + \frac{p}{\sqrt{1+p^2\phi^2+4pH}}, \tag{19}$$

where $p = p_1 = p_2$ and $\phi = \phi_1 = \phi_2$. The minimum value of $\chi_{\rm sp}$ corresponds to the critical point.

Let us take now explicitly the limits of high and low salt concentrations for the symmetric p case. The high-salt limit ($p \ll 1$) corresponds to the Debye-Hückel regime for which the spinodal line is given by

$$\chi_{\rm sp} \approx \frac{1}{2\phi(1-\phi)} + \frac{p}{1+4pH}, \tag{20}$$

and the critical point is located at $\chi_{\rm c} = 2, \phi_{\rm c} = 0.5$. This means that the bilayer behaves as if it were a neutral membrane when the salt concentration is sufficiently high.

In the other limit of low salt ($p \gg 1$), the spinodal line is given by

$$\chi_{\rm sp} \approx \frac{1}{2\phi(1-\phi)} + \frac{1}{\phi+4H}, \tag{21}$$

and it is independent of p. If the electrostatic coupling is weak enough ($H \ll 1$), the respective critical point is located at

$$\begin{aligned}\chi_{\rm c} &= (2+\sqrt{3})\left(1 - \frac{8H}{3}\right),\\ \phi_{\rm c} &= \frac{3-\sqrt{3}}{2} - \frac{4H(\sqrt{3}-1)}{3}.\end{aligned} \tag{22}$$

In the absence of the electrostatic coupling ($H = 0$), the critical point coincides with that in the previous works [18,19,22]:

$$\begin{aligned}\chi_{\rm c} &= 2+\sqrt{3} \simeq 3.73\,,\\ \phi_{\rm c} &= (3-\sqrt{3})/2 \simeq 0.634\,.\end{aligned} \tag{23}$$

III. GLOBAL PHASE DIAGRAMS AND CRITICAL BEHAVIOR

Based on the model described in the previous section, we present results for the critical point and phase diagrams in the case of two coupled and charged leaflets. In particular, we focus on the difference between a symmetric case in which the two solutions have the same ionic strength ($p_1 = p_2$) and the asymmetric case in which they differ ($p_1 \neq p_2$).

We start by giving some estimates for the physical choices of the parameter values of p_1, p_2, and H. The cross-sectional area of a lipid head group is set to about $\Sigma \simeq 65\,\text{Å}^2$ (taken to be the same for the two lipids), and the membrane thickness is $d \simeq 50\,\text{Å}$. From these values together with $\varepsilon_{\rm w} \simeq 80\varepsilon_0$, $\varepsilon_{\rm L} \simeq 3\varepsilon_0$ (ε_0 is the vacuum permittivity) and $T \simeq 300\,\text{K}$, we obtain $p \simeq 0.67\kappa^{-1}$ where κ^{-1} is measured in angstroms, and $H = 5.6\times10^{-4}$. In the following, we use a range of values $p = 0.5,5,50$ and extended the H range to cover $H = 0.005,0.01,0.05$. In the case of monovalent salt, the values $p = 0.5,5,50$ correspond, respectively, to $\kappa^{-1} = 0.75$, 7.5, 75 Å or to $n = 16\,\text{M}$, 160 mM, 1.6 mM. Since the electrostatic coupling parameter H is proportional to $\varepsilon_{\rm L}/d$, the larger H values correspond to smaller d and/or larger $\varepsilon_{\rm L}$. Obviously, the range in the p parameter of 10^2 gives a range of 10^4 in ionic strength, which probably is too large to compare with experiments. Hence it should be taken just to indicate trends with changing the salinity.

We show first the phase separation in asymmetric charged bilayers sandwiched between the two ionic solutions having the *same* ionic strength ($p_1 = p_2$), repeating the results of Ref. [18]. Then we present results for asymmetric charged leaflets that are in contact with two ionic solutions having *different* ionic strengths ($p_1 \neq p_2$).

A. Symmetric in/out reservoirs: $p_1 = p_2$

In Fig. 2 we show the critical interaction and composition $(\chi_{\rm c},\phi_{\rm c})$ as a function of p for the symmetric reservoir case, $p = p_1 = p_2$. Both $\chi_{\rm c}$ and $\phi_{\rm c}$ are obtained by numerically minimizing Eq. (19). The solid, dashed, dot-dashed lines correspond, respectively, to $H = 0.005,0.01$, and 0.05. The horizontal dotted lines located at $\chi_{\rm c} = 2+\sqrt{3} = 3.73$ and $\phi_{\rm c} = (3-\sqrt{3})/2 = 0.634$ are the critical values for the $H \to 0$ limit and for high-salt conditions.

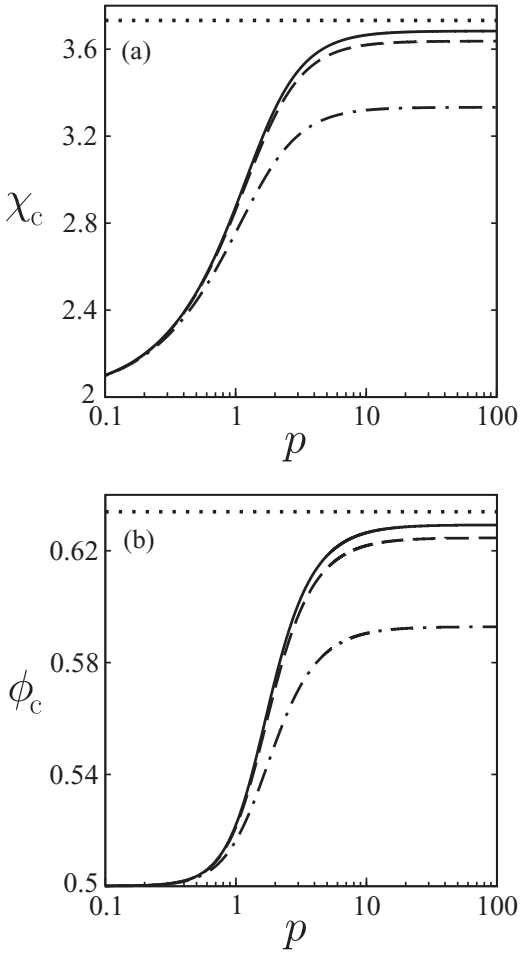

FIG. 2. (a) The critical interaction χ_c and (b) critical composition ϕ_c as a function of p on a semilog plot for different H values in the symmetric case ($p_1 = p_2 = p$). The solid, dashed, and dot-dashed lines are for $H = 0.005, 0.01, 0.05$, respectively. For $H = 0$, the critical values are represented by the dotted lines located at (a) $\chi_c = 2 + \sqrt{3} \simeq 3.73$ and (b) $\phi_c = (3 - \sqrt{3})/2 \simeq 0.634$.

When $\chi > \chi_c$, the membrane undergoes a lateral phase separation, whereas for $\chi < \chi_c$ the membrane is in a single (homogeneous) phase. For all H values, we find that χ_c becomes smaller as p decreases. Namely, the phase-separation temperature is increased, and the two-phase region has a larger extent for smaller p. This is because the Coulombic repulsion between the charged lipids becomes too weak to overpower the attractive interaction that drives the phase separation. When H is large, χ_c becomes much smaller, as will be discussed in Sec. IV. In the high-salt limit or when p is small enough, the limit of $\chi_c \to 2$ and $\phi_c \to 0.5$ can be seen, as was discussed in Sec. II. In the opposite low-salt limit, χ_c and ϕ_c approaches those of Eq. (22).

B. Asymmetric in and out reservoirs: $p_1 \neq p_2$

The calculated value of χ_c for the asymmetric case, in which the two solutions have different ionic strengths, is plotted in Fig. 3. Since χ_{sp} equals to χ_c at the critical point, χ_c is obtained by calculating numerically the minimum value of χ_{sp} via Eq. (14). The horizontal axis is the ratio p_2/p_1 in logarithmic scale, where $p_2/p_1 = 1$ corresponds to equal ionic strength of the two reservoirs. The solid, dashed, and dot-dashed lines denote fixed $p_1 = 0.5, 5$, and 50, respectively, while the coupling parameter H has three different values $H = 0.005, 0.01$, and 0.05 in the three figure parts. Similar to the findings of Fig. 2, χ_c decreases as the coupling H increases. This dependence of χ_c on H is similar as in the symmetric case and is further discussed in Sec. IV. In all plotted cases there is a peak around $p_2/p_1 = 1$, without a break in its slope there even for the solid line. For $p_2/p_1 < 1$, χ_c decreases as the salt concentration in solution 2 is increased, similar to the symmetric case.

Moreover, the Coulombic repulsion between charged lipids in the same leaflet becomes weak and χ_c decreases when p_2/p_1 becomes smaller. For $p_2/p_1 > 1$, χ_c is found to decrease and its value is more pronounced when H becomes larger, although the electrostatic screening is weaker. The physical origin of this behavior will be further discussed in Sec. IV.

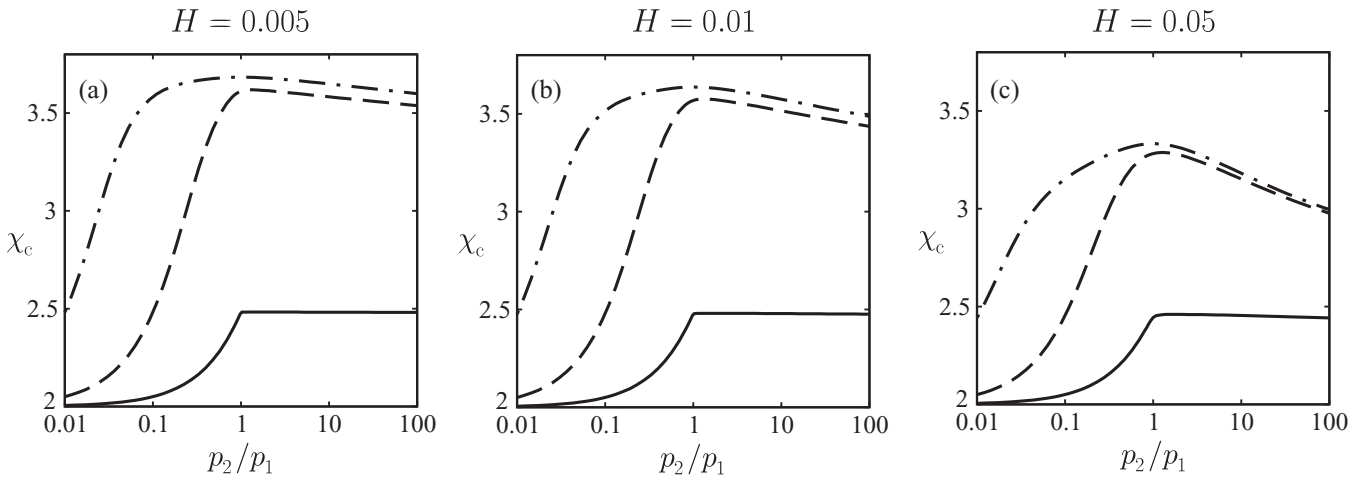

FIG. 3. The critical value χ_c as function of the asymmetry parameter, p_2/p_1, which also is equal to the ratio of the two Debye lengths, κ_1/κ_2. The solid, dashed, and dot-dashed lines are for $p_1 = 0.5, 5, 50$, respectively. The values of the H parameter are (a) $H = 0.005$, (b) $H = 0.01$, and (c) $H = 0.05$.

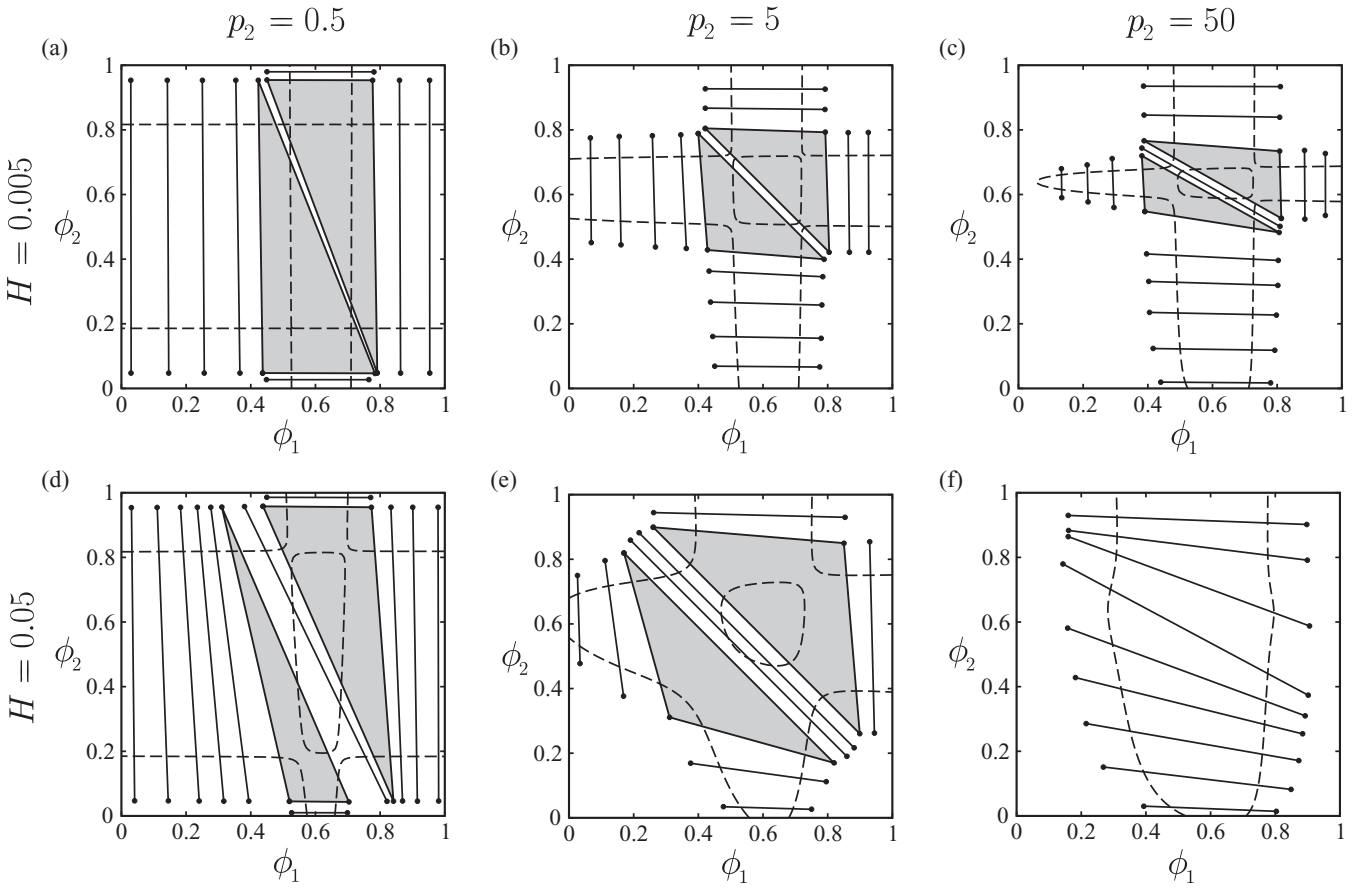

FIG. 4. Phase diagrams in the (ϕ_1,ϕ_2) plane for $\chi = 3.8$ and $p_1 = 5$. The solid lines are the tie lines and the dashed lines are the spinodal lines. The three-phase-coexistence regions are denoted by shaded triangles. The values of the other parameters are (a) $H = 0.005$ and $p_2 = 0.5$; (b) $H = 0.005$ and $p_2 = 5$; (c) $H = 0.005$ and $p_2 = 50$; (d) $H = 0.05$ and $p_2 = 0.5$; (e) $H = 0.05$ and $p_2 = 5$; and (f) $H = 0.05$ and $p_2 = 50$.

The calculated phase diagrams in the (ϕ_1,ϕ_2) plane for $\chi = 3.8$ and 4.0 are shown in Figs. 4 and 5, respectively. We plot all phase diagrams for a fixed $p_1 = 5$, while varying p_2 and H. As can be seen in Fig. 3, the system undergoes a phase separation for χ values larger than χ_c. The solid lines are the tie lines within the coexistence region, while the dashed lines correspond to the spinodal lines. Each pair of points connected by the tie line satisfies the conditions $\mu_{1,A} = \mu_{1,B}$, $\mu_{2,A} = \mu_{2,B}$ [Eq. (17)] and $g_A = g_B$ [Eq. (18)], while the spinodal lines are obtained from Eqs. (10), (14), and (16). In some of the figures, inner and external spinodal lines can be seen. However, the inner lines are preempted by the external ones. Since Fig. 4(b) and 4(e) and Fig. 5(b) and 5(e) are for the symmetric case ($p_1 = p_2$), these four phase diagrams are symmetric with respect to the diagonal line, $\phi_1 = \phi_2$. All other phase diagrams correspond to asymmetric situations, $p_1 \neq p_2$.

The phase-coexistence region becomes relatively larger when $p_2/p_1 \ll 1$, corresponding to strongly screened systems. However, χ_c for the asymmetric case is smaller than that of the symmetric case. When $H = 0.005$, most of the tie lines are nearly parallel to either ϕ_1 or ϕ_2 axis. This implies that the phase separation in each leaflet takes place almost independently and without any noticeable correlation with the second leaflet. On the other hand, for $H = 0.05$, the tie lines are tilted, indicating a strong coupling between the two leaflets.

The three-phase-coexistence regions are indicated by shaded triangles in the phase diagrams. The tie lines in the vicinity of the three-phase-coexistence regions are almost orthogonal to the principal diagonal $\phi_1 = \phi_2$, indicating that ϕ_1 is small when ϕ_2 is large and vice versa. This occurs when the local concentration of charged lipid in one of the leaflets is increased, while the concentration in the second leaflet is decreased conversely. This behavior is caused by the electrostatic coupling between the leaflets, as is discussed in the next section.

IV. DISCUSSION AND COMPARISON WITH EXPERIMENTS

Several points merit further discussion. First, we compare our theoretical results with experiments, where it was reported that the phase separation is enhanced when salt is added to charged bilayers [10]. Such a tendency is well reproduced in Figs. 4 and 5 when the salt concentration in solution 2 is increased or equivalently p_2 is decreased. A similar trend was also presented in previous works [12–14] for charged membranes without any electrostatic interleaflet coupling. In addition, it was reported by Vequi-Suplicy *et al.* [11] that the phase-separation temperature increases in the presence of salt.

In previous experimental studies [10,11], vesicles were first dispersed in the aqueous solution, and only then salt

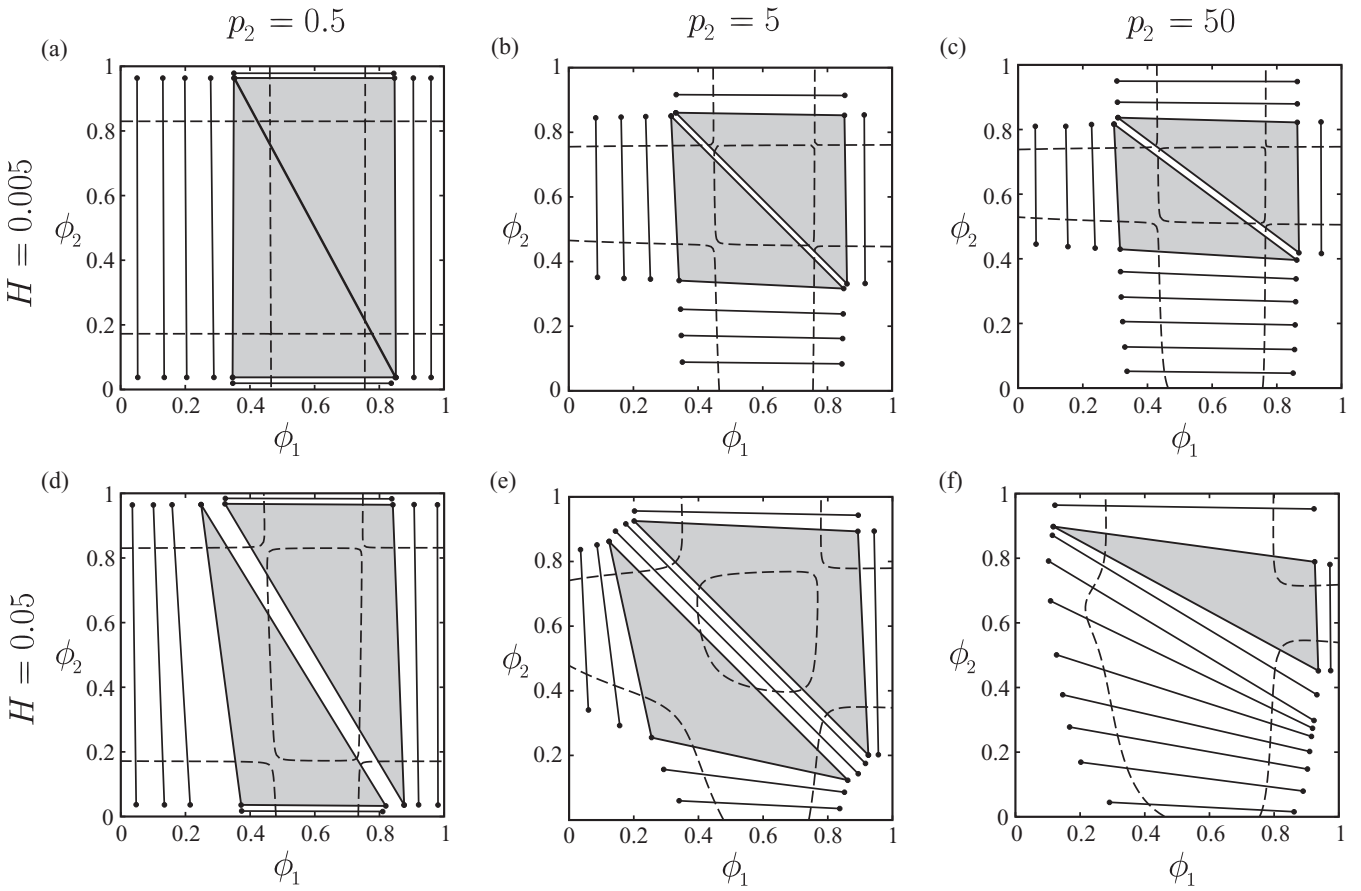

FIG. 5. Phase diagrams in the (ϕ_1,ϕ_2) plane for $\chi = 4.0$ and $p_1 = 5$. The solid lines are the tie lines, and the dashed lines are the spinodal lines. The three-phase-coexistence regions are denoted by shaded triangles. The values of the other parameters are (a) $H = 0.005$ and $p_2 = 0.5$; (b) $H = 0.005$ and $p_2 = 5$; (c) $H = 0.005$ and $p_2 = 50$; (d) $H = 0.05$ and $p_2 = 0.5$; (e) $H = 0.05$ and $p_2 = 5$; and (f) $H = 0.05$ and $p_2 = 50$.

was added, affecting only the ionic strength of the solution outside the vesicles. For this experimental procedure the value of p_2/p_1 is smaller than unity (recalling that p_2 corresponds to the outer reservoir). This situation is presented in Fig. 3 where $\chi_c \sim 1/T_c$ decreases as $p_2/p_1 < 1$ becomes smaller, in accord with the experimental observations. In addition, we find that also for $p_2/p_1 > 1$, χ_c is decreased even if the electrostatic screening is weak. In order to confirm this behavior in experiments, only the outer solution should be diluted in order to yield $p_2/p_1 > 1$. Controlled experiments done on asymmetric charged membranes with asymmetric in and out ionic strengths are needed to confirm the predictions of the present work. Because the lipid composition in each leaflet prepared by gentle hydration or electroformation is not well controlled, it is better to prepare vesicles by transferring water-in-oil droplets coated by lipids from an oil phase to a water phase [23,24] or by using asymmetric Montal-Mueller planar bilayers [15,25].

In the following, we discuss the physical reason why χ_c decreases for $p_2/p_1 > 1$. Such a tendency is more pronounced for larger $H \sim \varepsilon_L/d$, because the electrostatic coupling between the two leaflets becomes stronger. Notice that the electrostatic coupling depends on p_1 and p_2 as well as on H. As schematically presented in Fig. 6, the electrostatic coupling is weaker when the salt concentration in solution 2 is higher (upper panel of Fig. 6), and the phase separation is suppressed.

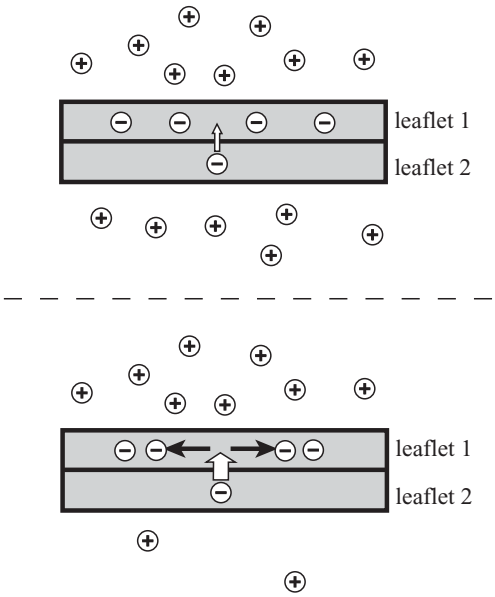

FIG. 6. Schematic illustration of the phase separation for an asymmetric charged lipid bilayer when $p_2/p_1 > 1$. On the upper panel, the salt concentration in solution 2 is high (but still obeying $p_2/p_1 > 1$). On the lower panel, the salinity in solution 2 is reduced resulting in an increase of p_2/p_1. The electrostatic coupling becomes then stronger and the phase separation is induced.

On the other hand, when the salt concentration in solution 2 is low (lower panel of Fig. 6), the screening is not as efficient, and phase separation is induced due to the strong electrostatic coupling. Note that in the latter case, the strong demixing in leaflet 1 is induced by changing the salt concentration in other reservoir (solution 2), which is coupled directly with the opposite leaflet. This is indeed an interesting situation because the higher salinity in solution 1 relative to 2 triggers the phase separation in leaflet 1 due to the strong interleaflet electrostatic coupling. The region where the tie lines are almost parallel to the ϕ_1 axis means that the phase separation mainly takes place in leaflet 1. As can be seen in Fig. 4(c) and 4(f) as well as in Fig. 5(c) and 5(f), such a region becomes much larger than the region where the phase separation strongly occur in leaflet 2 for large p_2. On the other hand, the phase separation also occurs in leaflet 2, although the concentration difference between two phases is very small. As shown in Fig. 3, χ_c is slightly decreased when p_1 is smaller and can be understood by noting that the screening sufficiently weakens the electrostatic coupling.

In Figs. 2 and 3 we have shown that χ_c is smaller for larger H, i.e., when the electrostatic interaction across the membrane is large. Because of the electrostatic coupling, the local charge accumulation in one of the two leaflets suppresses the charge accumulation in the other leaflet, and it is energetically unfavorable for the charged domains on each leaflet to face each other. As a result, a phase separation is induced in the other leaflet driven by the electrostatic coupling.

Next we elaborate on the physical meaning of the slope of the tie lines in Figs. 4 and 5. When the tie lines are located close to the three-phase region (triangle) and/or when H is large, the tie lines tend to be almost orthogonal to the principal diagonal. These tie lines connect two points on the binodal line that have a large compositional asymmetry between ϕ_1 and ϕ_2. It indicates that the charged domains in one leaflet do not prefer to face the charged domains in the other leaflet. The model by Baciu and May [18] as well as the present model deal with the compositional coupling between the two leaflets arising exclusively from electrostatic interactions. Consequently, it is energetically favorable for the charged domains on each leaflet not to face each other.

In order to see the contribution of the electrostatic coupling clearly, we consider the electrostatic coupling in the symmetric case ($p_1 = p_2$). The free energy of the interleaflet interaction $f_{\rm coup}$ is obtained by subtracting the contributions of individual leaflets from the total free energy

$$f_{\rm coup}(\phi_1,\phi_2) = f_{\rm tot}(\phi_1,\phi_2) - f_{\rm mix}(\phi_1) - f_{\rm mix}(\phi_2) - f_{\rm m}(\phi_1) - f_{\rm m}(\phi_2). \tag{24}$$

For small composition differences, the potential difference across the membrane is approximately given by

$$\Delta\Psi \approx -\frac{2p}{4Hp + \sqrt{1 + p^2\phi_{\rm av}^2}}(\phi_1 - \phi_2), \tag{25}$$

where $\phi_{\rm av} = (\phi_1 + \phi_2)/2$ is the average composition of the charged membrane. Substituting Eq. (25) into Eq. (24), we obtain an interleaflet free energy that can be expanded in terms of $\phi_1 - \phi_2$ [26],

$$f_{\rm coup}(\phi_1,\phi_2) \approx -\frac{2Hp^2}{1 + p^2\phi_{\rm av}^2 + 4Hp\sqrt{1 + p^2\phi_{\rm av}^2}}(\phi_1 - \phi_2)^2. \tag{26}$$

From Eq. (26), it is clear that $f_{\rm coup}$ is negative and becomes smaller when the difference between ϕ_1 and ϕ_2 is large, because the coefficient of $(\phi_1 - \phi_2)^2$ is negative. This is consistent with the tie lines in the phase diagrams, and a similar tendency can be seen even for the more general asymmetric systems.

In general, the physical origin of the coupling between the two leaflets can vary and does not have to rely exclusively on electrostatics interaction. Examples of such nonelectrostatic effects were considered in previous works [26,27] and include cholesterol flip-flop, dynamic chain interdigitation, van der Waals interaction or composition-curvature coupling. The coupling between the two leaflets can be expressed generally by

$$f_{\rm coup} = \Lambda(\phi_1 - \phi_2)^2 \tag{27}$$

as shown in Eq. (26). The coupling coefficient Λ becomes negative in the case of the electrostatic coupling. However, Wagner *et al.* [16] analyzed a model for coupled bilayers containing such a phenomenological term as in Eq. (27) but with $\Lambda > 0$. It is, therefore, important to consider the sign and typical value of Λ for different systems containing electrostatic and nonelectrostatic couplings and to reveal how the interactions between the two leaflets contribute to the coupling constant, Λ. Further experimental and theoretical investigations are required to gain more insight on this coupling and its origin.

The present work is concerned with macrophase separation in lipid membranes. Membranes consisting of neutral and charged lipids can form also modulated phases [28] that exhibit characteristic periodic structures. Hirose *et al.* [29] considered the coupling between two microphase separated bilayer leaflets. Various patterns, phases and their phase transitions were predicted by assuming a phenomenological coupling between the two leaflets.

We would like to close by mentioning again the two main approximations used in the present model. (1) We have treated the two leaflets as undeformable flat sheets. By doing so we neglected any possible bilayer deformation that can occur because of osmotic pressure difference resulting from a difference in ionic concentrations ($p_1 \neq p_2$) on the two membrane sides. In experiments, phase-separated domains produce budding toward the interior of the vesicle, and this is a direct consequence of the osmotic pressure on the spontaneous curvature [10]. In future studies it may be of advantage to consider the combined effect of the phase separation and membrane deformation. (2) We have used the Poisson-Boltzmann theory for symmetric monovalent salt in order to describe the electrostatic potential. It is known that such a mean-field theory does not treat correctly ion-ion correlation, especially when multivalent cations are involved. This important effect should also be taken into account in follow-up modeling.

In conclusion, we have considered the phase separation in a charged and asymmetric lipid bilayer, located between two ionic solutions having different ionic strengths. Considering the electrostatic effects on the phase separation, we have introduced the electrostatic coupling between the two leaflets. We studied the effect of the ionic strength difference between the two solutions, $p_1 \neq p_2$, and the electrostatic coupling H on the membrane phase behavior. When the electrostatic coupling H is introduced, $\chi_c \sim 1/T_c$ becomes smaller than for the uncoupled case. Moreover, even if the screening effect is small, χ_c decreases by increasing the asymmetry in the salt concentrations. An increase in the ionic strength leads to an enlarged coexistence region in the phase diagram.

ACKNOWLEDGMENTS

We are grateful to S. May and M. Schick for numerous comments and suggestions. NS was supported by a JSPS Research Fellowship for Young Scientists (23-8690) and Excellent Young Researchers Overseas Visit Program from the Ministry of Education, Culture, Sports, Science and Technology of Japan. This work was partially supported by KAKENHI (Grant-in-Aid for Scientific Research) on Priority Area "Soft Matter Physics," Grant No. 21540420 from the Ministry of Education, Culture, Sports, Science and Technology of Japan, the Israel Science Foundation (ISF) under grant no. 231/08, and the US-Israel Binational Science Foundation (BSF) under grant no. 2006/055.

APPENDIX: SURFACE POTENTIAL AND CHARGING FREE ENERGY OF AN ISOLATED LEAFLET

1. Leaflet electrostatic potential

We present the derivation of the surface potentials $\Psi_{1,2}$ [Eqs. (7) and (9)] and the electrostatic free energy of an isolated leaflet [Eq. (12)]. In order to find Ψ_1, we multiply the Poisson-Boltzmann equation (4) by $\psi_1'(z)$ and integrate it once, yielding

$$\int \psi_1' \psi_1'' \, dz = \kappa_1^2 \int \psi_1' \sinh \psi_1 \, dz, \tag{A1}$$

where $\psi_1' = d\psi_1/dz$ and $\psi_1'' = d^2\psi_1/dz^2$. Using the appropriate boundary conditions results in the following expression:

$$\psi_1' = -2\kappa_1 \sinh\left(\frac{\psi_1}{2}\right), \tag{A2}$$

and at $z = d$,

$$\psi_1'(d) = -2\kappa_1 \sinh\left(\frac{\Psi_1}{2}\right). \tag{A3}$$

Using Eq. (6) and $\psi_1'(d) = \psi_2'(0) = \Delta\Psi/d$, it follows that

$$\sinh\left(\frac{\Psi_1}{2}\right) = -\frac{2\pi\ell_B}{\kappa_1\Sigma}\phi_1 - \frac{2\pi\ell_B}{\kappa_1\Sigma}\frac{\Sigma}{4\pi\varepsilon_w\ell_B}\frac{\varepsilon_L}{d}\Delta\Psi. \tag{A4}$$

From this expression, the surface potential Ψ_1 is

$$\Psi_1 = -2\sinh^{-1}\left(p_1\phi_1 + p_1 H \Delta\Psi\right), \tag{A5}$$

where $p_1 = 2\pi\ell_B/\kappa_1\Sigma$, $H = \Sigma\varepsilon_L/4\pi\varepsilon_w\ell_B d$ as well as other parameters were introduced in Sec. II. The surface potential on the second leaflet, Ψ_2, can be obtained in the same way.

2. Electrostatic free energy of an isolated leaflet

Next we calculate the electrostatic free energy of an *isolated* leaflet, Eq. (12), using the charging method. A similar derivation can be found, e.g., in Refs. [19,21]. This energy corresponds to the energy that a leaflet feels in solution *without* the electrostatic coupling to the second leaflet. When a charged leaflet at $z = 0$ is in contact with an ionic solution situated at $z > 0$, the Poisson-Boltzmann equation gives

$$\psi' = -2\kappa \sinh\left(\frac{\psi}{2}\right). \tag{A6}$$

This equation is the same as Eq. (A2). The nonlinear first-order differential equation can then be integrated analytically:

$$\psi(z) = -2\ln\left\{1 + \frac{2}{\exp(\kappa z)\coth\left[\frac{1}{2}\sinh^{-1}(p\phi)\right] - 1}\right\}. \tag{A7}$$

From this expression, the surface potential $\Psi = \psi(z = 0)$ is given by

$$\Psi = -2\sinh^{-1}(p\phi). \tag{A8}$$

Through the charging process, the electrostatic free energy of an isolated leaflet is obtained by the following integral over Ψ yielding an analytical expression for f_m:

$$f_m(\phi) = -\int_0^\phi \Psi(s)\, ds = 2\phi\left\{\frac{1 - \sqrt{(p\phi)^2 + 1}}{p\phi} + \ln\left[p\phi + \sqrt{(p\phi)^2 + 1}\right]\right\}. \tag{A9}$$

[1] K. Simons and E. Ikonen, Nature (London) **387**, 569 (1997).
[2] S. L. Veatch and S. L. Keller, Phys. Rev. Lett. **89**, 268101 (2002).
[3] S. L. Veatch and S. L. Keller, Phys. Rev. Lett. **94**, 148101 (2005).
[4] T. Baumgart, S. T. Hess, and W. W. Webb, Nature (London) **425**, 821 (2003).
[5] S. L. Veatch and S. L. Keller, Biophys. J. **85**, 3074 (2003).
[6] S. Rozovsky, Y. Kaizuka, and J. T. Groves, J. Am. Chem. Soc. **127**, 36 (2005).
[7] R. Lipowsky and R. Dimova, J. Phys. Condens. Matter **15**, S31 (2003).
[8] S. Komura, N. Shimokawa, and D. Andelman, Langmuir **22**, 6771 (2006).
[9] G. G. Putzel and M. Schick, Biophys. J. **95**, 4756 (2008).
[10] N. Shimokawa, M. Hishida, H. Seto, and K. Yoshikawa, Chem. Phys. Lett. **496**, 59 (2010).
[11] C. C. Vequi-Suplicy, K. A. Riske, R. L. Knorr, and R. Dimova, Biochim. Biophys. Acta **1798**, 1338 (2010).

[12] S. May, D. Harries, and A. Ben-Shaul, Phys. Rev. Lett. **89**, 268102 (2002).
[13] D. Harries, S. May, and A. Ben-Shaul, Colloids Interfaces A **208**, 41 (2002).
[14] E. C. Mbamala, A. Ben-Shaul, and S. May, Biophys. J. **88**, 1702 (2005).
[15] M. D. Collins and S. L. Keller, Proc. Natl. Acad. Sci. USA **105**, 124 (2008).
[16] A. J. Wagner, S. Loew, and S. May, Biophys. J. **93**, 4268 (2007).
[17] G. G. Putzel and M. Schick, Biophys. J. **94**, 869 (2008).
[18] C. L. Baciu and S. May, J. Phys. Condens. Matter **16**, S2455 (2004).
[19] A. J. Wagner and S. May, Eur. Biophys. J. **36**, 293 (2007).
[20] E. J. W. Verwey and J. T. G. Overbeek, *Theory of the Stability of Lyophobic Colloids* (Elsevier, Amsterdam, 1948).
[21] D. F. Evans and H. Wennerström, *The Colloidal Domain* (John Wiley, New York, 1999).
[22] W. M. Gelbart and R. Bruinsma, Phys. Rev. E **55**, 831 (1997).
[23] S. Pautot, B. J. Frisken, and D. A. Weitz, Proc. Natl. Acad. Sci. USA **100**, 10718 (2003).
[24] T. Hamada, Y. Miura, Y. Komatsu, Y. Kishimoto, and M. Vestergaard, and M. Takagi, J. Phys. Chem. B **112**, 14678 (2008).
[25] M. Montal and P. Mueller, Proc. Natl. Acad. Sci. **69**, 3561 (1972).
[26] S. May, Soft Matter **5**, 3148 (2009).
[27] S. Leibler and D. Andelman, J. Phys. **48**, 2013 (1987).
[28] G. D. Guttman and D. Andelman, J. Phys. II **3**, 1411 (1993).
[29] Y. Hirose, S. Komura, and D. Andelman, Chem. Phys. Chem. **10**, 2839 (2009).